ISSN 0915-633X

INTERNATIONAL ATOMIC ENERGY AGENCY

18th IAEA Fusion Energy Conference
Sorrento, Italy, 4 to 10 October 2000

IAEA-CN-77/THP2/14

NATIONAL INSTITUTE FOR FUSION SCIENCE

Three Dimensional Ideal MHD Stability Analysis in *L=2* Heliotron Systems

N. Nakajima

(Received - Sep. 22, 2000)

NIFS-664 Oct. 2000

RESEARCH REPORT
NIFS Series

TOKI, JAPAN

Three dimensional ideal MHD stability analysis in $L = 2$ heliotron systems

N.Nakajima

National Institute for Fusion Science, Oroshi-cho 322-6, Toki, Japan 509-5292

e-mail: nakajima@nifs.ac.jp

Abstract. Global mode analyses of ideal MHD instability are performed under both fixed and free boundary conditions for $L/M = 2/10$ heliotron configurations, where L and M are the polarity and toroidal field period of helical coils, respectively. Under the fixed boundary condition, dangerous low-n ballooning modes with $n < M$ (n is a typical toroidal mode number) are not destabilized, when the pressure gradient almost vanishes near plasma periphery. However, such ballooning modes and/or peeling modes are destabilized under the free boundary condition even for the currentless condition, when a steep pressure gradient exists near the plasma boundary. Effects of the net toroidal current on the external modes are also discussed.

1. Introduction

Ideal MHD stability analyses in $L = 2$ heliotron systems with a large Shafranov shift ($M \sim 10$), represented by LHD and CHS, have been performed mainly for pressure-driven interchange modes, taking account of feasibility of currentless operations, where L and M are the polarity and toroidal field period of helical coils, respectively The local mode analyses for modes with a short wave length ($n \to \infty$) based on the Mercier criterion and the two dimensional global mode analyses for modes with a finite wave length ($n < M$) based on the stellarator-expansion have been done, where n is toroidal mode number. The results of the global mode analyses are consistent with those of the local mode analyses. In contrast with them, both ballooning modes and external modes have not been examined intensively. The reason is that the global ballooning modes in three dimensional systems can not be constructed in terms of the results of the local mode analysis in the ballooning space, and hence the local mode analysis merely gives the conjecture about the properties of global modes [1, 2]. Recently, for the Mercier-unstable MHD equilibria, the conjecture from the local ballooning mode analysis has been proved [3]. On the other hand, feasibility of currentless operations puts obstacles on the free boundary global mode analysis of the external modes thought to be mainly driven by a net toroidal current, so that only the two dimensional global mode analysis has been done recently [4].

The purpose of this article is to prove the conjecture from the local ballooning mode analysis in the Mercier-stable equilibria through the three dimensional global mode analysis, and to perform the three dimensional free boundary global mode analysis for external modes, in order to systematically clarify both their properties and influences on MHD equilibria. MHD equilibria are calculated under the fixed boundary condition by using VMEC [5], whose vacuum configuration is similar to the LHD standard configuration [6]. Only pressure and toroidal current profiles are changed to control MHD equilibria. Global analyses are done by using CAS3D [7].

2. Local Mode Analysis

For convenience, the results of the local mode analysis are summarized here. The unstable eigenvalues ω^2 in the local mode analysis of the ballooning modes are the function of ψ, θ_k, and α, where ψ and α are the labels of the flux surface and the magnetic field line in the ballooning space, respectively, and θ_k is the radial wave number stemming from the eikonal approximation. In Mercier-unstable equilibria, the unstable eigenvalues $\omega^2(< 0)$ have two types of topological level surfaces in (ψ, θ_k, α) space. One is cylindrical level surface with the axis along α direction. The other is spheroidal level surface,

which exists inside of the cylindrical level surfaces. Only spheroidal level surfaces exist in Mercier-stable equilibria. From those, it is conjectured that [2]

1. Global modes that correspond to modes in the local mode analysis with a topologically cylindrical level surface for ω^2 will be poloidally localized tokamak-like ballooning modes or interchange modes. Effects of the toroidal mode coupling on these modes are weak.
2. Global modes corresponding to modes in the local mode analysis with a topologically spheroidal level surface for ω^2 will be such ballooning modes inherent to three-dimensional systems with strong toroidal mode coupling that they have high poloidal and toroidal mode numbers and are localized in both the poloidal and toroidal directions. These modes become to be localized within each toroidal field period of the helical coils, as their typical toroidal mode numbers become higher.
3. For Mercier-unstable equilibria, where both topologically cylindrical and spheroidal level surfaces for ω^2 coexist, poloidally localized tokamak-like ballooning modes or interchange modes with weak toroidal mode coupling appear when their typical toroidal mode numbers are relatively low. As the typical toroidal mode numbers become higher, such ballooning modes inherent to three-dimensional systems appear with strong toroidal mode coupling that they have larger growth rates and are localized in both the poloidal and toroidal directions.
4. In Mercier-stable equilibria, where only a topologically spheroidal level surface for ω^2 exists, only such ballooning modes inherent to three-dimensional systems appear with strong toroidal mode coupling that they have high poloidal and toroidal mode numbers and are localized in both the poloidal and toroidal directions.

3. Fixed Boundary Global Mode Analysis

Three dimensional equilibria are categorized into two types; toroidicity-dominant equilibria with strong reduction of the local magnetic shear, and helicity-dominant ones with weak reduction. The former is obtained by a peaked pressure profiles and/or a net toroidal current decreasing the rotational transform ι, which create a large Shafranov shift, and the latter is made by a broader pressure profiles and/or a net toroidal current increasing ι, leading to a small Shafranov shift.

3.1 Mercier-unstable Equilibria

The toroidicity-dominant Mercier-unstable equilibrium is created with the peaked pressure profile $P = P_0(1 - \psi_N)^2$ with $\beta_0 = 5.9\%$, under the flux conserving condition, where ψ_N and β_0 are the normalized toroidal flux and the beta value at the magnetic axis, respectively. Note that the normalized radial coordinate is given by $r_N = \sqrt{\psi_N}$. The helicity-dominant one is created with the broad pressure profile $P = P_0(1 - \psi_N^2)^2$ with $\beta_0 = 4\%$, under the currentless condition. The results of the global mode analysis are consistent with the conjecture from the local mode analysis, as are indicated in Tab. 1. Unstable modes occur in the plasma periphery with stellarator-like magnetic shear and the averaged unfavorable magnetic curvature, where the Mercier criterion is violated [3].

	toroidicity-dominant	*helicity-dominant*
$n < M$	interchange modes with negligible toroidal mode couplings	interchange modes with negligible toroidal mode couplings
$n \sim M$	tokamak-like ballooning modes with weak toroidal mode couplings	interchange modes with weak toroidal mode couplings
$n \gg M$	3D ballooning modes with strong toroidal mode couplings	3D ballooning modes with strong toroidal mode couplings

Tab. 1 Most unstable modes in Mercier-unstable MHD equilibria

3.2 Mercier-stable Equilibrium

The Mercier-stable equilibria belong to the toroidicity-dominant equilibria, one of which is created with the peaked pressure profile $P = P_0(1 - \psi_N)^2$ with $\beta_0 = 8\%$, under the currentless condition. The global mode analysis has newly proved the conjecture from the local ballooning mode analysis as summarized in Tab. 2. Unstable modes localize in the plasma periphery with stellarator-like magnetic shear and the averaged unfavorable magnetic curvature as well as in Mercier-unstable equilibria.

$n < M$	stable
$n \sim M$	3D ballooning modes with strong toroidal mode couplings
$n \gg M$	3D ballooning modes with strong toroidal mode couplings

Tab. 2 Most unstable modes in Mercier-stable MHD equilibria

The magnetic curvature consists of two parts: one is due to toroidicity, and the other is due to helicity of helical coils. $L = 2$ heliotrons have an elliptic poloidal cross section held between two helical coils. On the outer side of the torus, the magnetic curvature is locally unfavorable on the horizontally elongated poloidal cross section and it is locally favorable on the vertically elongated poloidal cross section. From this variation of the local magnetic curvature along the toroidal direction, low-n ballooning modes ($n < M$) with a long wave length in the toroidal direction are not destabilized. In the contrast with them, ballooning modes with moderate ($n \sim M$) and high ($n \gg M$) toroidal mode numbers can be destabilized, because they could utilize the local magnetic curvature due to helicity through the strong toroidal mode couplings. Figs. 1 and 2 show the radial Fourier mode structure of the radial displacement $\vec{\xi} \cdot \nabla\psi$ of three dimensional ballooning modes and the corresponding typical toroidal mode numbers for $n \sim M$ and $n \gg M$, respectively. There are four (in Fig. 1) and six (in Fig. 2) groups of Fourier modes with different toroidal mode numbers through a strong toroidal mode coupling. The groups of Fourier modes with higher toroidal mode numbers exist in the region with higher rotational transform, and neighboring groups of Fourier modes have opposite phase to each other. This relative phase difference of the neighboring groups leads to the clear localization of the perturbed pressure in the toroidal direction. On the outer side of the torus, the perturbed pressure, which localizes on the horizontally elongated poloidal cross section with the locally unfavorable magnetic curvature at the outside of the torus, almost disappears on the vertically elongated poloidal cross section with the locally favorable magnetic curvature at the outside of the torus. Moreover, the strong toroidal mode coupling causes localization into flux tubes.

From above results for internal modes, it may be concluded that :

1. Dangerous low-n ballooning modes ($n < M$) with a large growth rate and a global radial profile are not destabilized when the pressure gradient almost vanishes near the plasma periphery.
2. Most unstable high-n instabilities are three dimensional ballooning modes, which may be considered to affect the marginal pressure gradient and the transport locally.

Note that for high-n ballooning modes, kinetic stabilizing effects (ion diamagnetic frequency, finite Larmor radius) should be taken into account.

4. Free Boundary Global Mode Analysis

In three-dimensional equilibria, the basic rotational transform is created by the external helical coil system, so that an amount of net toroidal current needed in tokamaks is not required. Thus, external modes are thought to be driven by the free energy near the plasma boundary. There are two types of free energy near the plasma boundary: one is due to the pressure gradient, namely Pfirsch-Schlüter current, and the other is due to a net toroidal current. Hereafter, effects of the vacuum vessel are ignored, namely, the wall exists infinitely away from the plasma boundary.

4.1 Pressure-driven modes

MHD equilibria used in the global mode analyses for the internal modes have almost no free energy near the plasma boundary, because the pressure gradient is quite small there, so that external modes are stable in these equilibria. In order to introduce the free energy due to the pressure gradient, a pressure profile with a steep gradient near the boundary is used: $P = P_0(1 - \psi_N)$ with $\beta_0 = 8\%$, under the currentless condition. The rotational transform at the plasma boundary is $\iota_b = 1.116$. This equilibrium has a Mercier unstable region near the plasma periphery, however, it is stable or slightly unstable against low-n interchange modes, under the fixed boundary condition. One of them is shown in Fig. 3, where each Fourier mode of the interchange mode is strongly localized around the mode rational surface. Under the free boundary condition, however, the mode structure is significantly changed into a tokamak-like ballooning mode as is shown in Fig. 4. Also, the growth rate is about ten times larger than that of the interchange mode under the fixed boundary condition. In the free boundary case, each Fourier component of $\vec{\xi} \cdot \nabla\psi$ may have a finite value at the plasma boundary. This fact allows the radial structure to decay slowly from the mode rational surface to the boundary, which enable for the Fourier modes to overlap in the radial direction, leading to a ballooning structure. Also, near the plasma periphery the averaged magnetic curvature is always unfavorable and Mercier unstable, so that not a three-dimensional but a two-dimensional (tokamak-like) ballooning modes are destabilized. When the typical toroidal mode number is increased, there is a possibility that a Fourier mode has the resonant surface just outside of the boundary. In such a case, most unstable modes changes from the tokamak-like ballooning modes into peeling modes [8], as is shown in Fig. 5.

4.2 Current-driven modes

In order to consider the current-driven free boundary modes, pressure profile without free energy near the plasma periphery is used: $P = P_0(1 - \psi_N)^2$ with $\beta_0 = 8\%$. As a current profile, two types of current profile are used: $J = J_0\psi_N^6(1 - \psi_N)$ with $I_P = 200(\mathrm{kA})$, and $J = J_0\psi_N^6$ with $I_P = 200(\mathrm{kA})$, where J is the net toroidal current density, and I_P is the total toroidal current. These currents decrease the rotational transform at the plasma boundary, so that $\iota_b < 1$. The peeling modes appear as in Fig. 6. The current profiles and the total amount of the net current are unlikely to occur, so that the current-driven external modes are irrelevant to realistic operation.

5. Conclusion

When the pressure gradient near the plasma boundary is small, dangerous low-n ballooning modes are stable independent of the boundary condition, however, when the pressure gradient becomes large, tokamak-like low-n ballooning modes and/or peeling modes may occur as external modes, which determine the maximum pressure gradient near the plasma boundary.

References

[1] Nakajima, N., Phys. Plasmas **3**, (1997) 4545.
[2] Nakajima, N., Phys. Plasmas **3**, (1997) 4556.
[3] Chen, J., Nakajima, N., and Okamoto, M., Phys. Plasmas **5**, (1999) 1562.
[4] Johnson, J. L., Ichiguchi, K., *et al.*, Phys. Plasmas **6**, (1999) 2513.
[5] Hirshman, S. P., Phys. Fluids **26**, (1983) 3553.
[6] Iiyoshi, A., *et al.*, Fusion Technol. **17**, (1990) 148.
[7] Schwab, C., Phys. Fluids B **5**, (1993) 3195.
[8] Lortz, D., Nucl. Fusion **15**, (1975) 49.

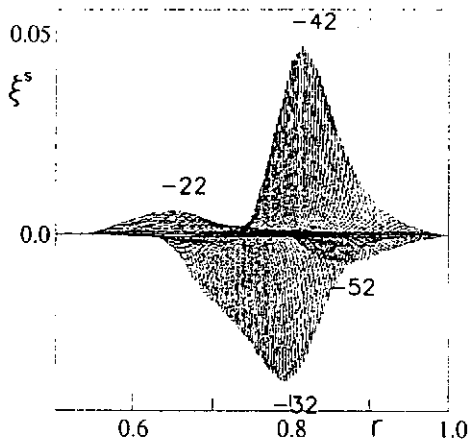

Fig. 1: Radial Fourier mode structure of $\vec{\xi} \cdot \nabla\psi$ with the dominant toroidal mode numbers (three dimensional ballooning mode with $n \sim M$).

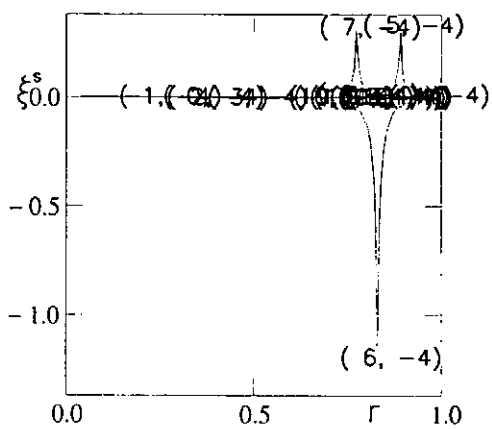

Fig. 3: Radial Fourier mode structure of $\vec{\xi} \cdot \nabla\psi$ with mode numbers (m, n), under the fixed boundary condition (interchange).

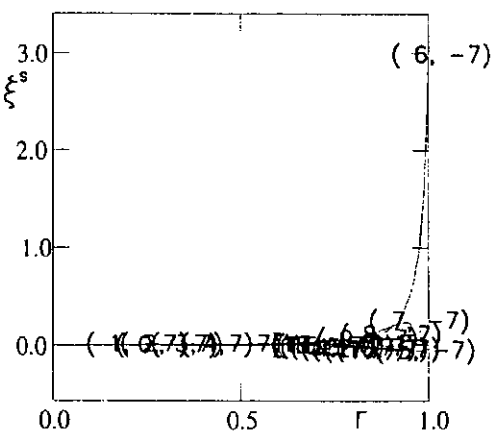

Fig. 5: The same quantities as in Fig. 3 under the free boundary condition (pressure-driven peeling mode) in the currentless equilibrium.

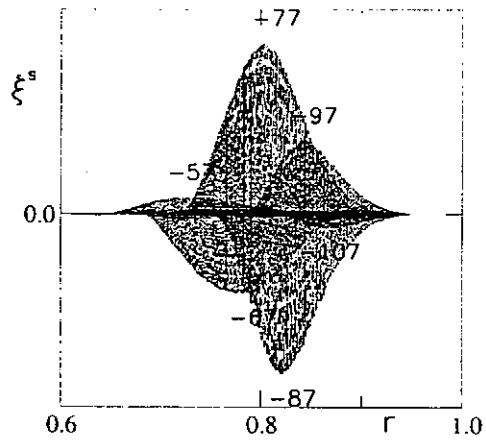

Fig. 2: The same quantities as in Fig. 1 for a ballooning mode with $n \gg M$.

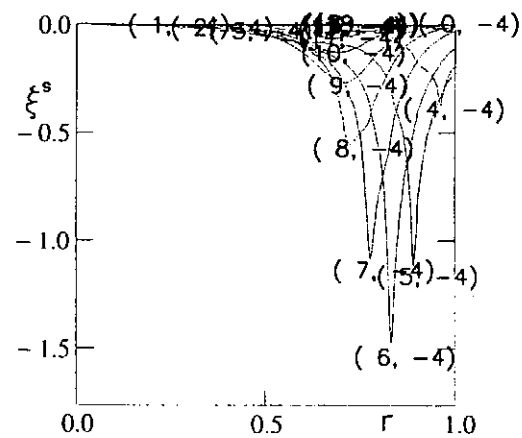

Fig. 4: The same quantities as in Fig. 3 for the free boundary condition (tokamak-like ballooning modes).

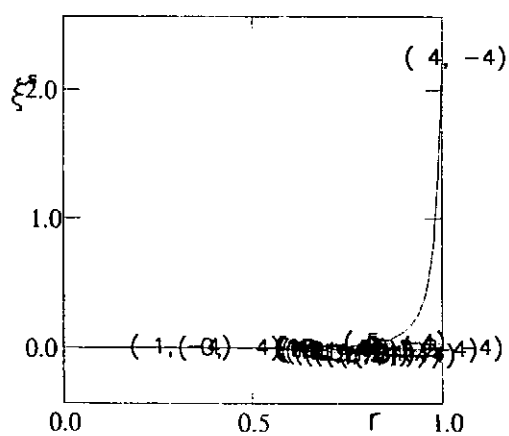

Fig. 6: The same quantities as in Fig. 3 under the free boundary condition (current-driven peeling mode) in the equilibrium with $J = J_0\psi_N^6$.

Recent Issues of NIFS Series

NIFS-657 M. Sasao, S. Murakami, M. Isobe, A.V. Krasilnikov, S. Iiduka, K. Itoh, N. Nakajima, M. Osakabe, K.Saito,T. Seki, Y.Takeiri, T. Watari, N.Ashikawa , P.deVaries, M.Emoto, H.Funaba, M.Goto, K.Ida, H.Idei, K.Ikeda, S.Inagaki, N.Inoue, S.Kado, O.Kaneko, K.Kawahata, K.Khlopenkov, T.Kobuchi , A.Komori, S.Kubo, R.Kumazawa, S.Masuzaki, T.Minami, J.Miyazawa, T.Morisaki, S.Morita, S.Muto, T.Mutoh, Y.Nagayama, Y.Nakamura, H.Nakanishi, K.Narihara, K.Nishimura, N.Noda, T.Notake, Y.Liang , S.Ohdachi, N.Ohyabu, Y.Oka, T.Ozaki, R.O.Pavlichenko, B.J.Peterson, A.Sagara, S.Sakakibara, R.Sakamoto, H.Sasao4, K.Sato, M.Sato, T.Shimozuma, M.Shoji, H.Suzuki, M.Takechi, N.Tamura, K.Tanaka, K.Toi, T.Tokuzawa, Y.Torii, K.Tsumori, H.Yamada, I.Yamada, S.Yamaguchi, S.Yamamoto, M.Yokoyama, Y.Yoshimura, K.Y.Watanabe and O. Motojima,
Study of Energetic Ion Transport in the Large Helical Device: Sep. 2000
(IAEA-CN-77/EX9/1)

NIFS-658 B.J.Peterson, Y.Nakamura, K.Yamazaki, N.Noda, J.Rice, Y.Takeiri, M.Goto, K.Narihara, K.Tanaka, K.Sato, S.Masuzaki, S.Sakakibara, K.Ida, H.Funaba, M.Shoji, M.Osakabe, M.Sato, Yuhong Xu, T.Kobuchi, N.Ashikawa, P.deVries, M.Emoto, H.Idei, K.Ikeda, S.Inagaki, N.Inoue, M.Isobe, S.Kado, K.Khlopenkov, S.Kubo, R.Kumazawa, T.Minami, J.Miyazawa, T.Morisaki, S.Murakami, S.Muto, T.Mutoh, Y.Nagayama, H.Nakanishi, K.Nishimura, T.Notake, Y.Liang, S.Ohdachi, Y.Oka, T.Ozaki, R.O.Pavlichenko, A.Sagara, K.Saito, R.Sakamoto, H.Sasao, M.Sasao, T.Seki, T.Shimozuma, H.Suzuki, M.Takechi, N.Tamura, K.Toi, T.Tokuzawa, Y.Torii, K.Tsumori, I.Yamada, S.Yamaguchi, S.Yamamoto, M.Yokoyama, Y.Yoshimura, K.Y.Watanabe, T.Watari, K.Kawahata, O.Kaneko, N.Ohyabu, H.Yamada, A.Komori, S.Sudo, O.Motojima
Impurity transport induced oscillations in LHD: Sep. 2000
(IAEA-CN-77/EXP5/27)

NIFS-659 T. Satow, S. Imagawa, N. Yanagi, K. Takahata, T. Mito, S. Yamada, H.Chikaraishi, A. Nishimura, I. Ohtake, Y. Nakamura, S. Satoh, O. Motojima,
Achieved Capability of the Superconducting Magnet system for the Large Helical Device: Sep. 2000
(IAEA-CN-77/FTP1/15)

NIFS-660 T. Watari, T. Mutoh, R. Kumazawa, T. Seki, K. Saito, Y. Torii , Y.P. Zhao , D. Hartmann , H. Idei, S. Kubo, K. Ohkubo, M. Sato, T. Shimozuma, Y. Yoshimura, K. Ikeda, O. Kaneko, Y. Oka, M. Osakabe, Y. Takeiri, K. Tsumori, N.Ashikawa , P.C.deVries, M. Emoto, A.Fukuyama , H. Funaba, M. Goto, K. Ida, S. Inagaki, N. Inoue, M. Isobe, K. Itoh, S. Kado, K. Kawahata, T. Kobuchi, K.Khlopenkov, A. Komori, A. Krasilnikov , Y.Liang,S. Masuzaki, K. Matsuoka, T. Minami, J. Miyazawa, T. Morisaki, S. Morita, S. Murakami, S. Muto, Y. Nagayama, Y. Nakamura, H. Nakanishi, K. Narihara, K. Nishimura, N. Noda, A. T.Notake, S. Ohdachi, N. Ohyabu, H. Okada , M. Okamoto, T. Ozaki, R.O.Pavlichenko, B.J. Peterson, A. Sagara, S. Sakakibara, R. Sakamoto, H. Sasao, M. Sasao, K. Sato, S. Satoh, T. Satow, M. Shoji, S. Sudo, H. Suzuki, M.Takechi, N.Tamura ,S. Tanahashi, K. Tanaka, K. Toi, T. Tokuzawa, K.Y. Watanabe, T. Watanabe, H. Yamada, I. Yamada, S. Yamaguchi, S.Yamamoto, K. Yamazaki, M.Yokoyama, Y. Hamada, O. Motojima, M. Fujiwara,
The Performance of ICRF Heated Plasmas in LHD : Sep. 2000
(IAEA-CN-77/EX8/4)

NIFS-661 K. Yamazaki, K. Y. Watanabe, A. Sagara, H. Yamada, S. Sakakibara, K. Narihara, K. Tanaka, M. Osakabe, K. Nishimura, O. Motojima, M. Fujiwara, the LHD Group,
Helical Reactor Design Studies Based on New Confinement Scalings : Sep. 2000
(IAEA-CN-77/ FTP 2/12)

NIFS-662 T. Hayashi, N. Mizuguchi, H. Miura and T. Sato,
Dynamics of Relaxation Phenomena in Spherical Tokamak : Sep.. 2000
(IAEA-CN-77THP2/13)

NIFS-663 H. Nakamura and T. Sato, H. Kambe and K. Sawada and T. Saiki,
Design and Optimization of Tapered Structure of Near-field Fiber Probe Based on FDTD Simulation: Oct. 2000

NIFS-664 N. Nakajima,
Three Dimensional Ideal MHD Stability Analysis in *L=2* Heliotron Systems: Oct. 2000
(IAEA-CN-77/THP2/14)